

Le Commandant Charcot

**GOOD-OARS-IMDOS**

Cruise O030622, O150622, O240622, O280622

O030622 (3 – 15 June 2022), O150622 (15 – 23 June 2022),  
O240622 (24 – 28 June), O280622 (28 June – 8 July 2022),  
Reykjavik (Iceland) – Longyearbyen, Svalbard (Norway)  
GOOD-OARS-IMDOS



**lead PI: Andreas Oeschlies**  
**GEOMAR**

Contributors to cruise report:  
Andreas Oeschlies, Veronique Garçon, Aaron Beck, Jan Taucher

**Table of Contents**

1	Cruise Summary
1.1	Summary in English
2	Participants
2.1	Principal Investigators
2.2	Scientific Party
2.3	Participating Institutions
3	Research Program
3.1	Description of the Work Area
3.2	Aims of the Cruise
3.2	Agenda of the Cruise
4	Narrative of the Cruise
5	Preliminary Results: CTD and water column sampling
5.1	Water Sampling with CTD and Niskin bottles
5.2	Particles and zooplankton (Underwater Vision Profiler 6)
6	Preliminary results: Microplastic distribution and composition
7	Overview of stations and sampling activities
8	Data and Sample Storage and Availability
9	Acknowledgements
10	References

## **1 Cruise Summary**

### **1.1 Summary in English**

The cruise consisted of 4 cruise legs, O030622 (3 – 15 June 2022, Reykjavik - Longyearbyen), O150622 (15 – 23 June 2022, Longyearbyen - Longyearbyen), O240622 (24 – 28 June, Longyearbyen - Longyearbyen), O280622 (28 June – 8 July 2022, Longyearbyen - Longyearbyen) in late northern spring into the Atlantic sector of the Arctic (Fig. 3.1). PONANT Science offered 4 berths as “Ship of Opportunity” on the new cruise expedition vessel “Le Commandant Charcot”, specially designed for extreme polar conditions.

On the first leg the ship sailed from Reykjavik along the eastern coast of Greenland with unusually intense sea ice cover and crossed Fram Strait to reach Svalbard. Three successive legs were operating in waters around Svalbard. With extraordinary support from the ship’s crew, 1-2 stations were typically carried out per day (Fig. 3.1), often on the shelf, but with several off-shelf deep water stations covering the southward flowing East Greenland Current and the northward flowing West Spitsbergen Current. CTD, dissolved oxygen, bulk particulate matter and optical Video Underwater Vision Profiler 6 (UVP6) measurements were taken at the stations. Whenever ice-free water was present at the stations, Manta net microplastic samples were obtained from a zodiac during 3 successive 20 minute sections. Data are currently analyzed and will be used to better constrain models of marine oxygen dynamics. An improved understanding of oxygen dynamics in polar waters that source large parts of the deep ocean should help resolving the discrepancies between relatively low rates of deoxygenation in current climate models and considerably higher rates in observational estimates.

## **2 Participants**

### **2.1 Principal Investigators**

<b>Name</b>	<b>Institution</b>
Oschlies, Andreas, Prof.	GEOMAR
Garçon, Véronique, Dr.	LEGOS, CNRS

### **2.2 Scientific Party**

<b>Name</b>	<b>Discipline</b>	<b>Institution</b>
Oschlies, Andreas, Prof.	Marine Biogeochemistry	GEOMAR
Parouffe, Alexandra	Marine Biogeochemistry	LEGOS, UPS
Taucher, Jan, Dr.	Marine Biogeochemistry	GEOMAR
Beck, Aaron, Dr.	Marine Biogeochemistry	GEOMAR

Savy, Jean-Philippe, Dr.	Marine Biogeochemistry	BORDEAUX
Ruiz Girona, Julia	Marine Biogeochemistry	LEGOS, IRD
Paul, Allannah, Dr.	Marine Biogeochemistry	GEOMAR
Stoll, Deborah	Marine Biogeochemistry	GEOMAR
Garçon, Veronique, Dr.	Marine Biogeochemistry	LEGOS, CNRS
Thielecke, Antonia	Marine Biogeochemistry	GEOMAR

### 2.3 Participating Institutions

GEOMAR Helmholtz-Zentrum für Ozeanforschung Kiel

LEGOS Laboratoire d'Etudes en Géophysique et Océanographie Spatiales, Toulouse,

CNRS Centre national de la recherche scientifique

BORDEAUX University of Bordeaux

## 3 Research Program

### 3.1 Description of the Work Area

Work area was the Arctic sector of the Atlantic, north of Iceland, along the eastern coast of Greenland and around Svalbard.

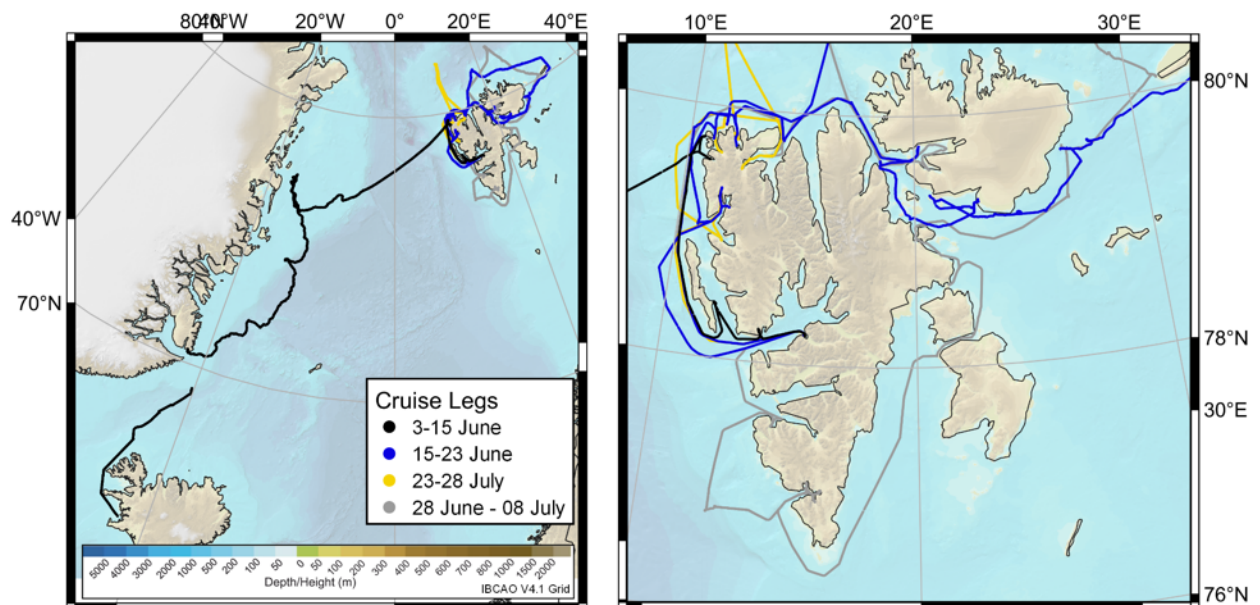


**Fig. 3.1:** Overview of work area and different cruise legs

### **3.2 Aims of the Cruise**

Field work focused on the role of climate change and ocean pollution in the Atlantic sector of the Arctic Ocean, in particular on the extent and mechanisms of deoxygenation and acidification and the resulting impacts on marine ecosystems.

### **3.3 Agenda of the Cruise**

Measurements taken are a contribution to the UN Decade of Ocean Science for Sustainable Development endorsed programmes GOOD (Global Ocean Oxygen Decade), OARS (Ocean Acidification Research for Sustainability), and those of the Global Ocean Observing System (GOOS, here focusing on expanding global observations of marine litter as part of the Integrated Marine Debris Observing System, IMDOS).

## **4 Narrative of the Cruise**

The cruise track of leg 1 covered a latitudinal gradient from 68°N (off Iceland) to 81°N (off Svalbard), in which most of the northward movement was along the Greenland coast. A particularity was that the Arctic sea ice coverage in 2022 was rather large (compared to the development of the last decades), so that *Le Commandant Charcot* traveled through largely intact sea ice on its way North (Fig. 4.1). Additional 3 legs were carried out surrounding Svalbard, mostly focusing on the fjords. In total, 30 stations for scientific sampling were conducted over the course of the 4 cruise legs (see section 7, station list).

As only a hand winch and a 1000m long rope were available, one of the electric winches on the aft deck of the ship was chosen to assist in the heaving. Speed was about 0.7m per second. A boom was constructed to ensure some distance of the instruments and samples from the ship's hull.

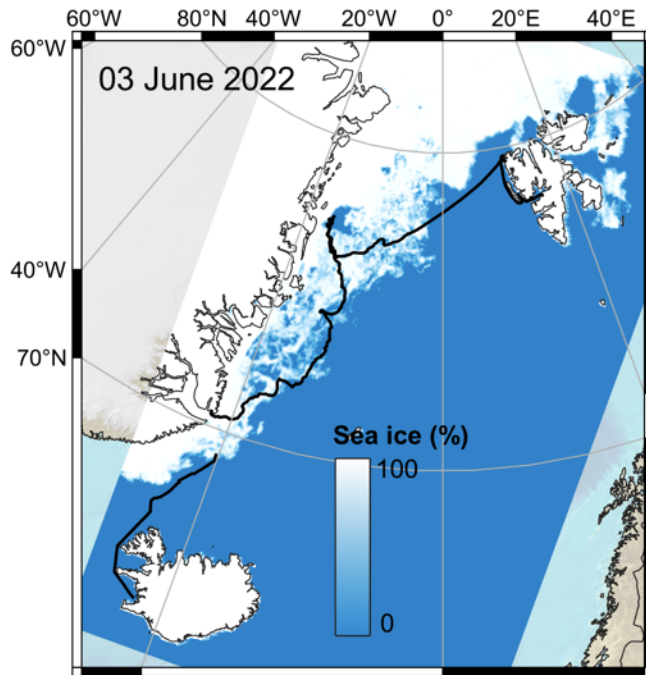


**Fig. 4.1:** Sea Ice coverage and concentration on cruise leg 1 as detected from satellite data on June 3rd 2022 (Source: NASA Worldview)

CTD, UVP and Niskin bottle stations:

On all sampling stations, a CTD, UVP6 (camera profiler) and Niskin bottles were deployed from the ship's aft to collect vertically resolved data of physical parameters (CTD), particles and zooplankton (UVP6), as well as biogeochemical key parameters such as chlorophyll and particulate carbon (see section 7, station list).

During the first two stations the CTD was not recording data – it might have been too cold on the aft deck, so that we decided to keep the CTD in the warmer interior of the ship until briefly before deployment. No problems occurred after adoption of this protocol.

## 5 Preliminary Results

### 5.1 Water Sampling with CTD and Niskin bottles

#### Hydrography and oxygen

During the 4 cruise legs, vertical profiles with a CTD incl. sensors for oxygen and turbidity were obtained on a total of 30 sampling stations. In addition to oxygen measurements from the CTD-mounted sensor, we took water samples at discrete depths with Niskin bottles and measured dissolved oxygen concentrations with the Winkler method. This data will help to calibrate the sensor-based oxygen data.

The first successful CTD deployment was at station 3 on 5<sup>th</sup> June, off the Greenland shelf break down to a depth of about 450m (Fig. 5.1). Clearly visible in the temperature profile are the cold and fresh Polar Surface Waters (PSW) and underlying warm ( $> 1^{\circ}\text{C}$ ) and saltier Recirculating

Atlantic Waters (RAW) between about 300m and 400m. Oxygen values decline from about 353  $\mu\text{M}$  at the surface to minimum values of 290  $\mu\text{M}$  at the centre of the RAW layer, corresponding to a minimum in saturation level of less than 84% (Fig. 5.1, 5.4).

On 6<sup>th</sup> June and between 9 and 11<sup>th</sup> June, daily stations were taken on the Greenland Shelf. On 8<sup>th</sup> June, another station (Station 5) could be taken down to 900m off the Greenland Shelf, featuring warm and salty RAW at a shallower depth of only 100 - 180m (Fig. 5.1). Further north, at Station 10 on 12<sup>th</sup> June at the western end of Fram Strait, the salty RAW core is shallower (180 – 340m), substantially warmer (up to 2.5°C), but contains only slightly higher concentrations of oxygen (295  $\mu\text{M}$ ) (Fig. 5.1, 5.3). On the eastern end of Fram Strait, warm Atlantic surface water is found with temperatures exceeding 4°C, in sharp contrast to freezing temperature close to -1.5°C less than 100 miles further west. There is surprisingly little difference in oxygen concentrations between stations 10 and 11 at the western and eastern end of Fram Strait, though saturation levels are generally lower at the warmer eastern end.

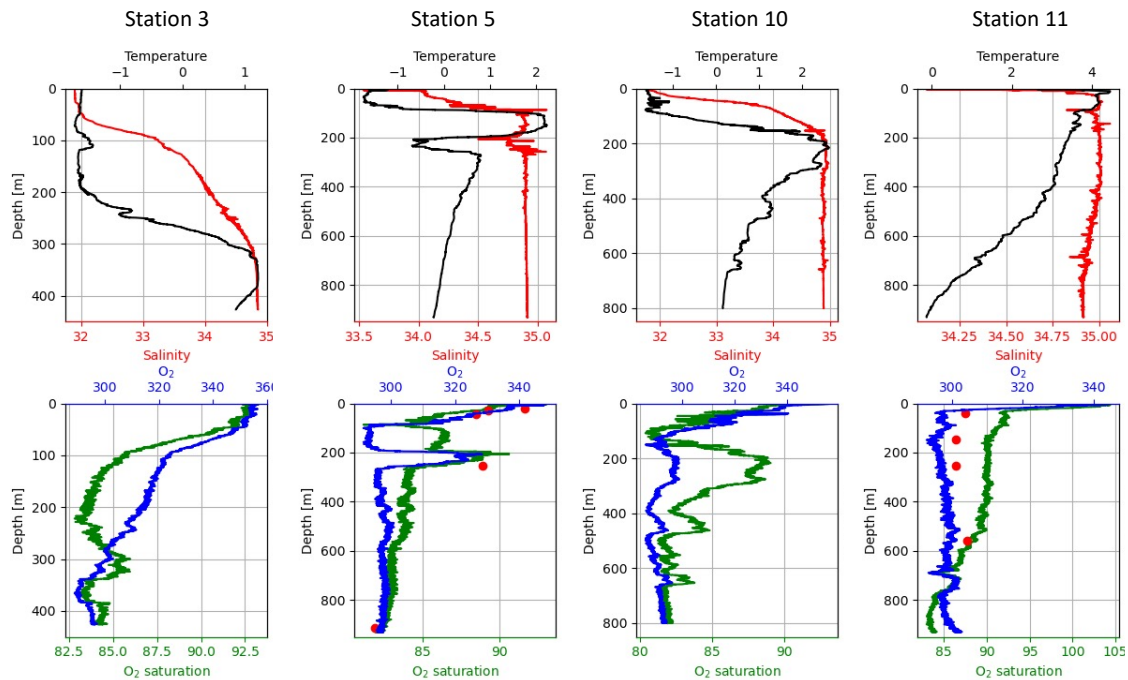


**Fig. 5.1.:** Hydrography at selected (deep water) stations during leg 1 (Iceland-Greenland-Svalbard).

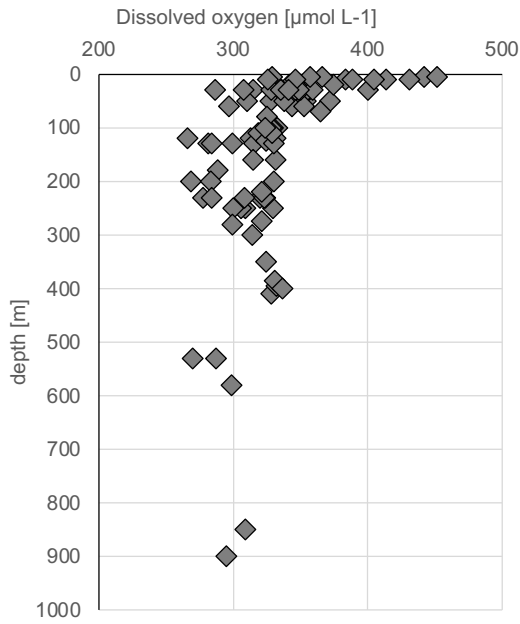


**Fig. 5.2.:** Overview of oxygen concentrations measured from Niskin sampling and Winkler titration (data from all cruise legs).

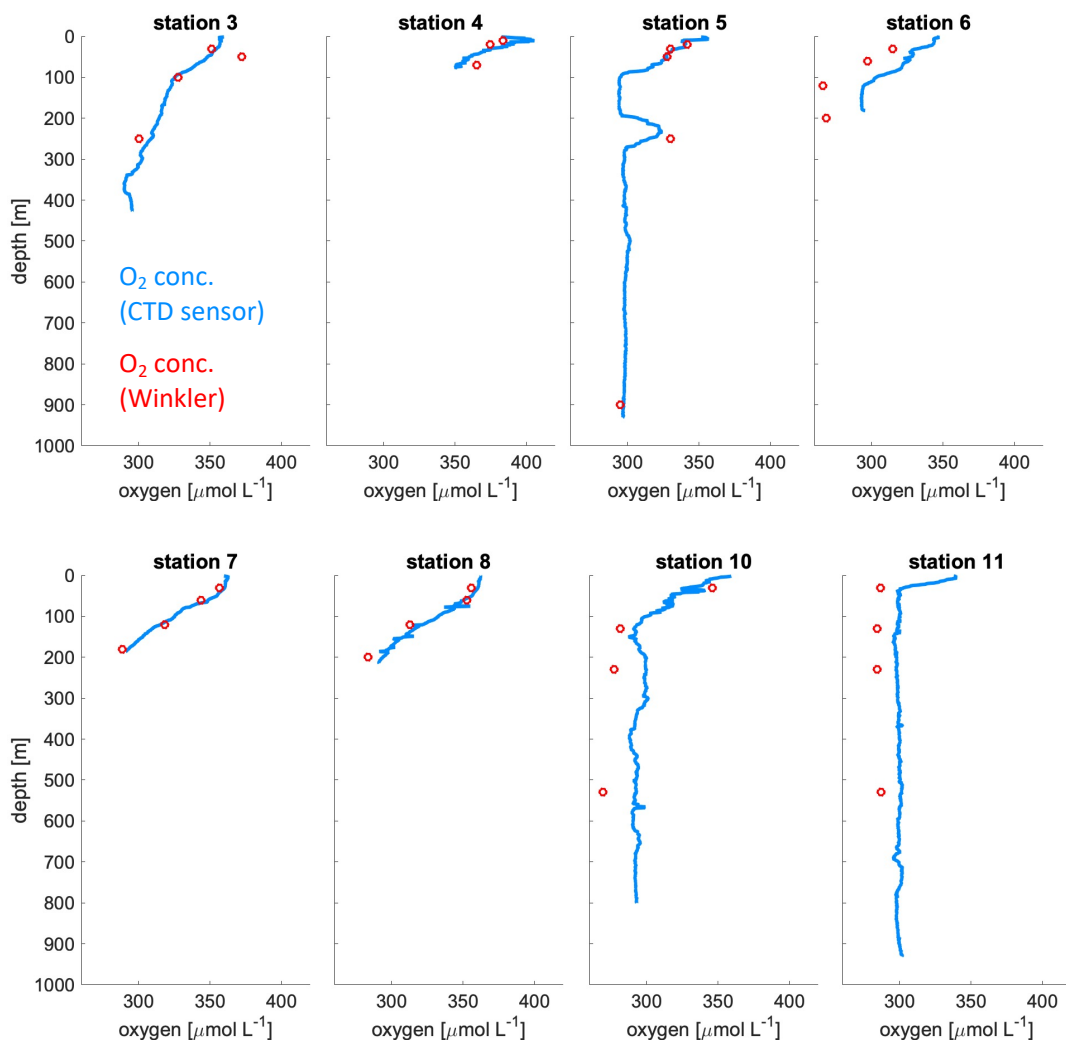




**Fig. 5.3.:** Overview of oxygen concentrations on stations of leg 1 (Iceland-Greenland-Svalbard) measured by CTD (blue lines) and Niskin (red circles), and oxygen saturation from CTD (green lines).

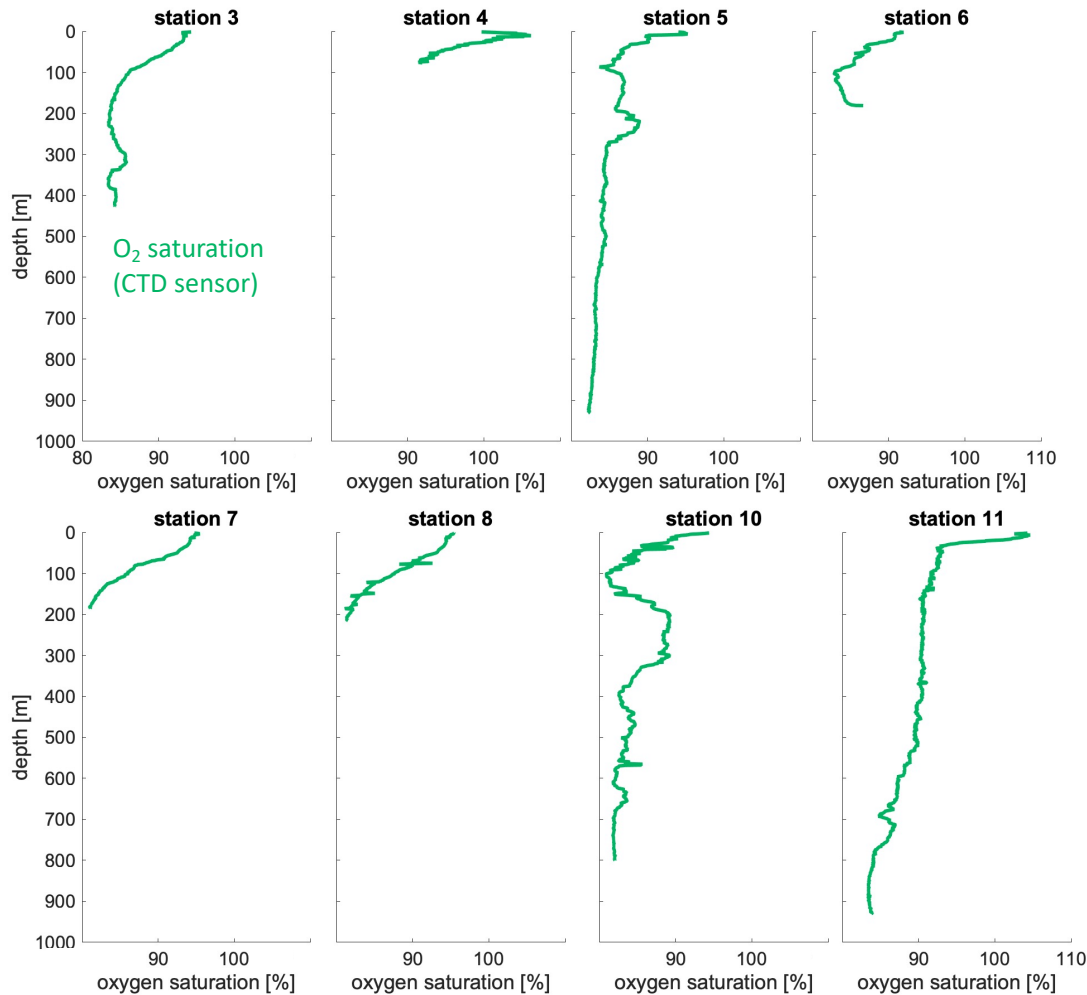


**Fig. 5.4.:** Overview of oxygen saturation on stations of leg 1 (Iceland-Greenland-Svalbard) measured by CTD.

An unexpected result were the relatively low oxygen saturation levels often below 95% saturation in the surface layers of the East Greenland Current (Stations 5 -10), which are in direct contact with the atmosphere and experience active primary production as evidenced by a high abundance of living phytoplankton and zooplankton. Such low surface concentrations are not currently simulated by our global climate models at any time during the seasonal cycle in ice-free waters of the Atlantic sector of the Arctic, which might partially explain why current models appear to underestimate the rate of decline in deep ocean oxygen concentrations. Sensitivity simulations with our models are currently performed at GEOMAR to understand if specific meteorological and sea-ice conditions in spring of 2022 could be responsible for the data-model discrepancy. It will also be interesting to see if similarly low oxygen concentrations in the surface waters will be measured on the follow-on cruise in 2023.

### **Chlorophyll and particulate organic matter**

Chlorophyll *a* concentrations were rather low, but variable, ranging between approx. 0.1 to 7  $\mu\text{g L}^{-1}$  (Fig. 5.5). In the surface layer (here: upper 100 m) most values concentrations were  $<0.5 \mu\text{g L}^{-1}$ . Some elevated values at intermediate depths indicate sinking of fresh phytodetritus.

Particulate organic carbon (POC) concentrations displayed the typical exponential with depth (Fig. 5.5), decreasing from maximum values of  $\sim 50 \mu\text{mol C L}^{-1}$  near the surface to values around  $10 \mu\text{mol L}^{-1}$  or less at depths  $>100\text{m}$ . Notably, molar C:N ratios were elevated compared to the canonical Redfield ratio of 6.6. The average C:N ratio of all samples was 10.2, and the highest frequency was found for C:N ratios between 8 and 9. There was no relationship between C:N and depth, which would indicate preferential remineralization of N over C.

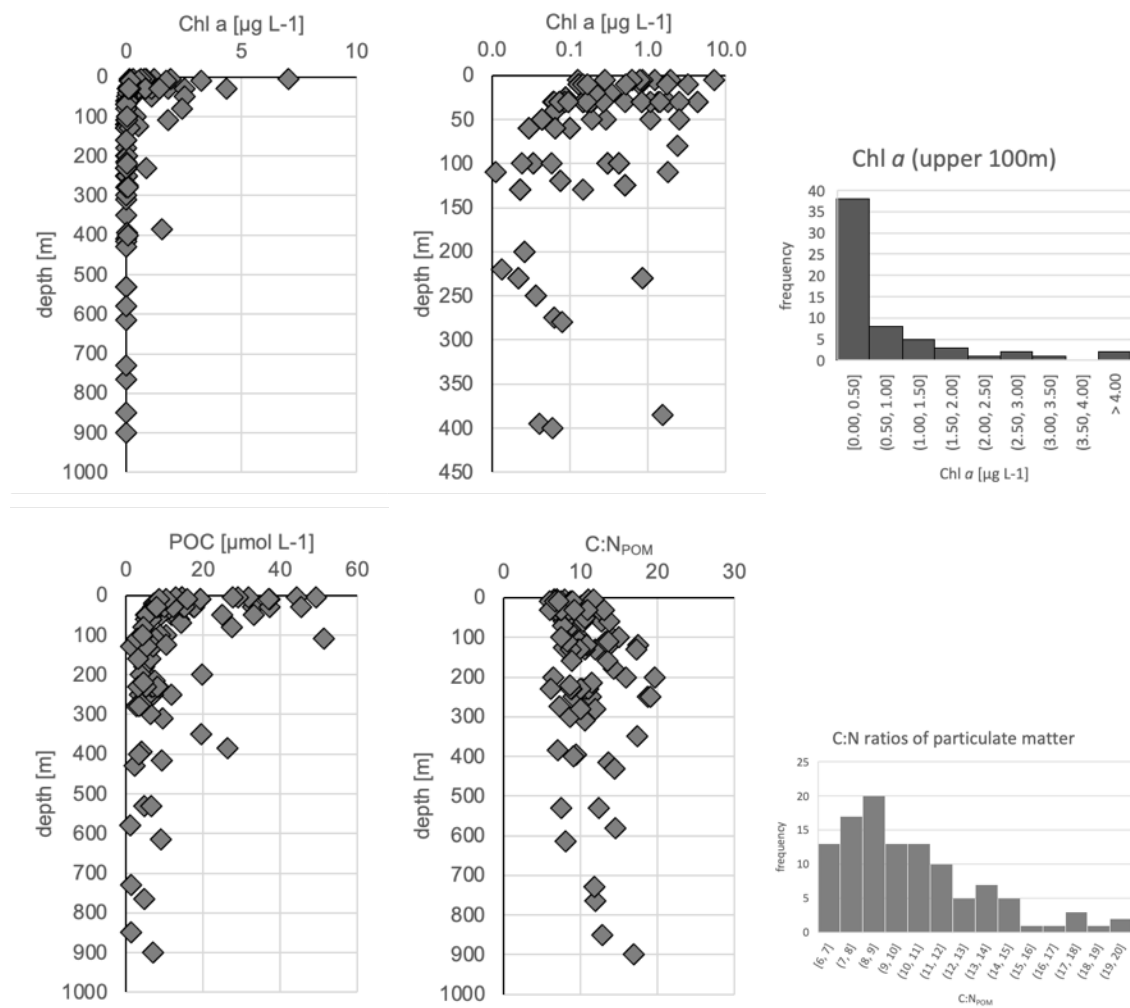


**Fig. 5.5:** Vertical profiles of chlorophyll *a* (upper row) and particulate organic carbon (POC; lower row) concentrations, summary of all cruise legs.

### **5.2. Particles and zooplankton (Underwater Vision Profiler 6)**

The Underwater Vision Profiler 6 (UVP6) is a special underwater camera system that collects images of particles and plankton during vertical profiles (Picheral et al. 2021). The UVP6 captured images at  $\sim 10 \text{ Hz}$  with a pixel resolution of  $73 \mu\text{m}$  in an imaged volume of  $\sim 600 \text{ ml}$ , thus allowing

to image and identify particles of organisms between approx. 1 to 100 mm (Fig. 5.6). Collected data were processed with the UVPapp software (provided by the manufacturer Hydroptic), including automated segmentation of “regions of interests” from raw images, and estimating their size (based on the number of pixels and geometric calculations).

Presently, data analysis is in the final phase, including classification of all detected organisms into taxonomic groups, and estimating their biovolume and its vertical profiles in the water column. Final data should be available in spring/summer 2023 and provided on the “EcoTaxa” platform, an plankton imaging database that collects data from all UVP units and provides them to the scientific community.

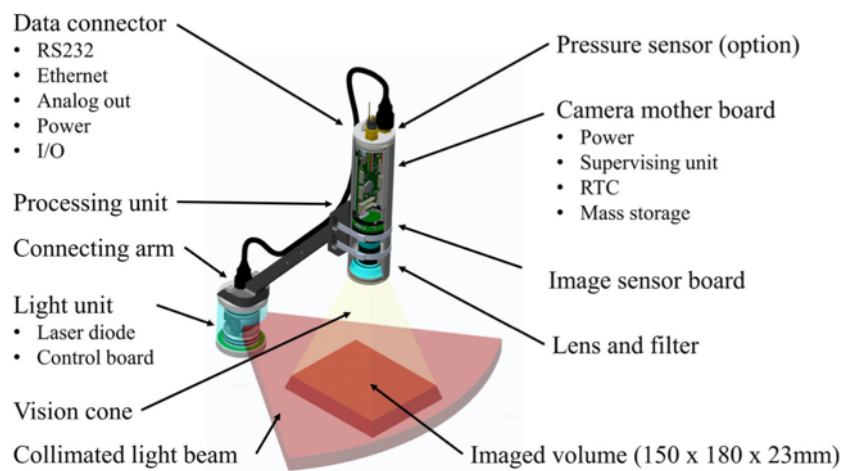
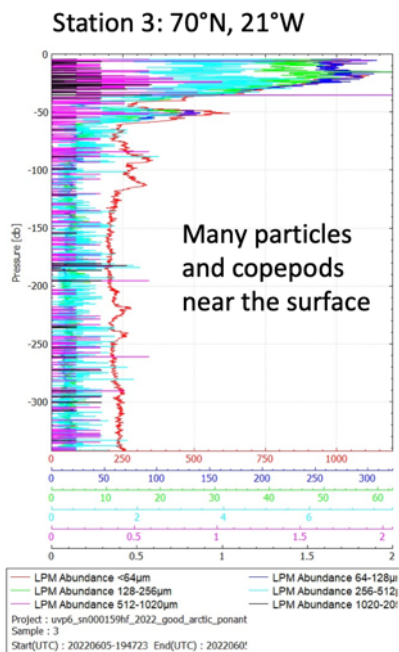


**Fig. 5.6:** Diagram of the UVP6 underwater camera

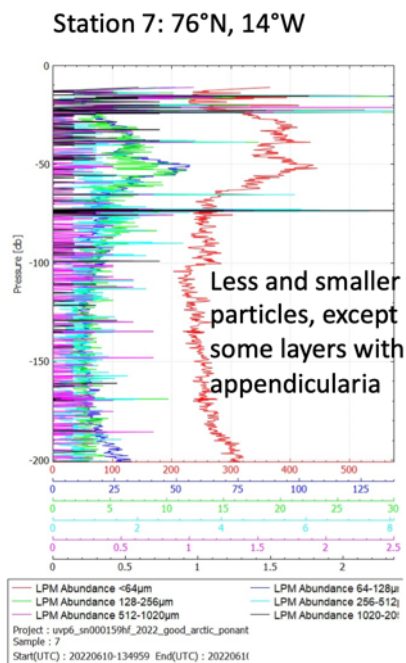
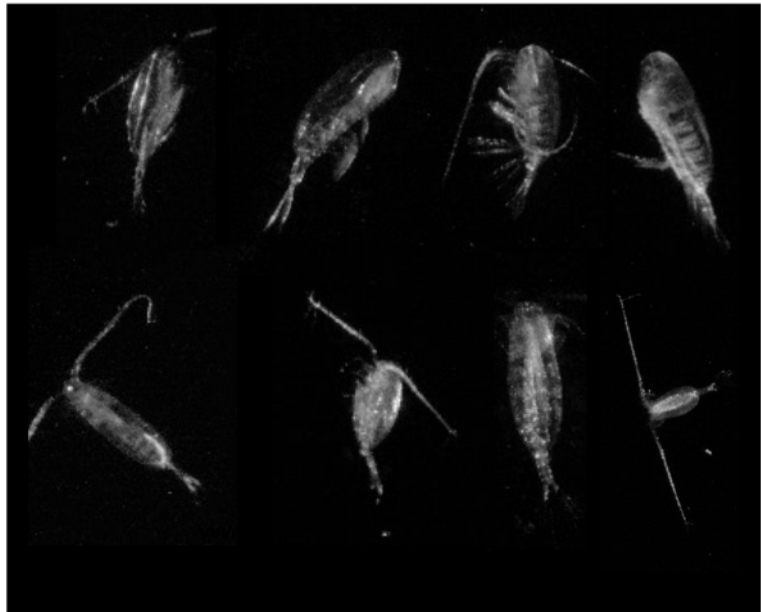
We mounted the UVP6 together with the CTD to collect vertically resolved data on all stations during leg 1 and 2. Preliminary analysis of data suggests a distinct spatial gradient in zooplankton abundance and taxonomic composition, with higher copepod abundances in southern stations, and lower overall abundances at more northern stations (including a shift from copepods to gelatinous taxa such as appendicularia; see Fig. 5.7). This gradient was likely related to seasonality i.e. particularly sea-ice coverage: Stations between Iceland until the Southeast Greenland coast were ice-free, whereas stations along the East Greenland shelf were still subject to a widely closed sea-ice cover (see Fig. 4.1).

Likely, the seasonal cycle was more advanced towards lower-latitude stations, with the spring/summer phytoplankton bloom already starting, and thus providing food for copepod populations. At higher latitudes (and higher sea-ice cover) we suspect that the phytoplankton bloom was not in progress yet, and thereby copepod populations were still low (or overwintering at greater depths than sampled). Zooplankton abundances were much lower here, and appendicularia (filter-feeding gelatinous plankton) were the dominant taxon. Their populations were likely sustained by elevated concentrations of small particles (< 60 µm), which is in their preferred prey size range.

The chlorophyll/pigment and POC/PON data (see 5.2) will help in interpreting zooplankton data in upcoming data analysis (mid/end 2023) and supporting/rejecting the hypothesis for the spatial differences outlined above.



Mostly copepods



Mostly appendicularia (gelatinous filter-feeders)

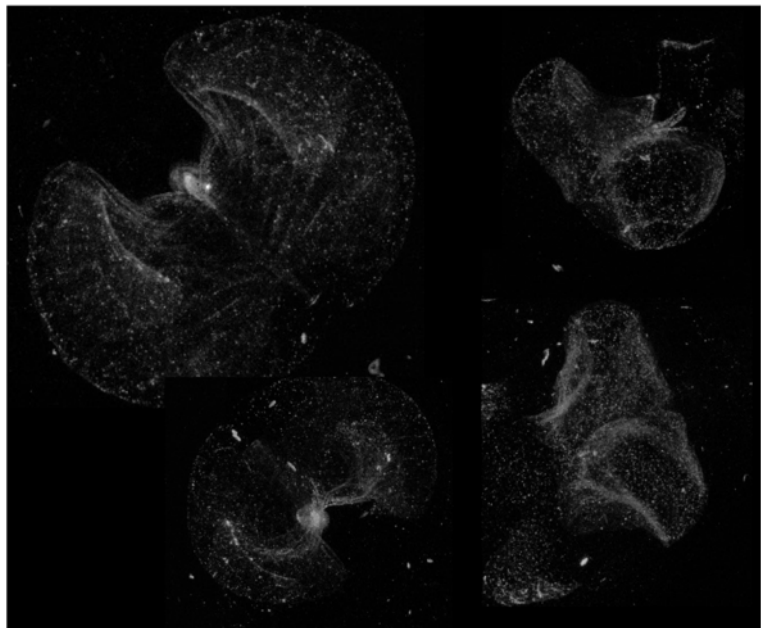


**Fig. 5.7:** Vertical profiles of UVP6 data at two contrasting sites during leg 1, off Southeast Greenland (low sea-ice cover) and between Greenland and Iceland (high sea-ice cover).

## 6. Preliminary results: Microplastic distribution and composition

A.J. Beck and D. Stoll (GEOMAR)

### Methods

Microplastic samples were collected from the ship's clean seawater supply and from manta net tows deployed from a rubber dinghy. The underway seawater supply (UWS; intake at ~10 m depth) was filtered through sequential stainless-steel filter sieves with mesh sizes of 1 and 300  $\mu\text{m}$ . The total volume sampled was recorded with an inline flow meter. A total of 29 UWS samples were collected across three cruise legs (Fig. 1; note that station UWS-6 does not exist). The seawater supply pump was turned off while the ship was traveling in pack ice due to clogging of the intake, so no UWS samples were collected in ice-covered regions except within ice-free polynyas. The flow rate was approximately 12 L/min, representing a filtered volume of between 1.5 and 20 m<sup>3</sup> (average  $6.5 \pm 3.7$  m<sup>3</sup>). Sieve samples were rinsed to one edge of the sieve with filtered seawater, and the concentrated particles transferred to a petri dish. Particles were visually identified under a dissecting scope or magnifying glass; all apparently non-natural particles were selected for imaging, as well as a representative selection of natural particles (e.g., copepod or pteropod individuals).

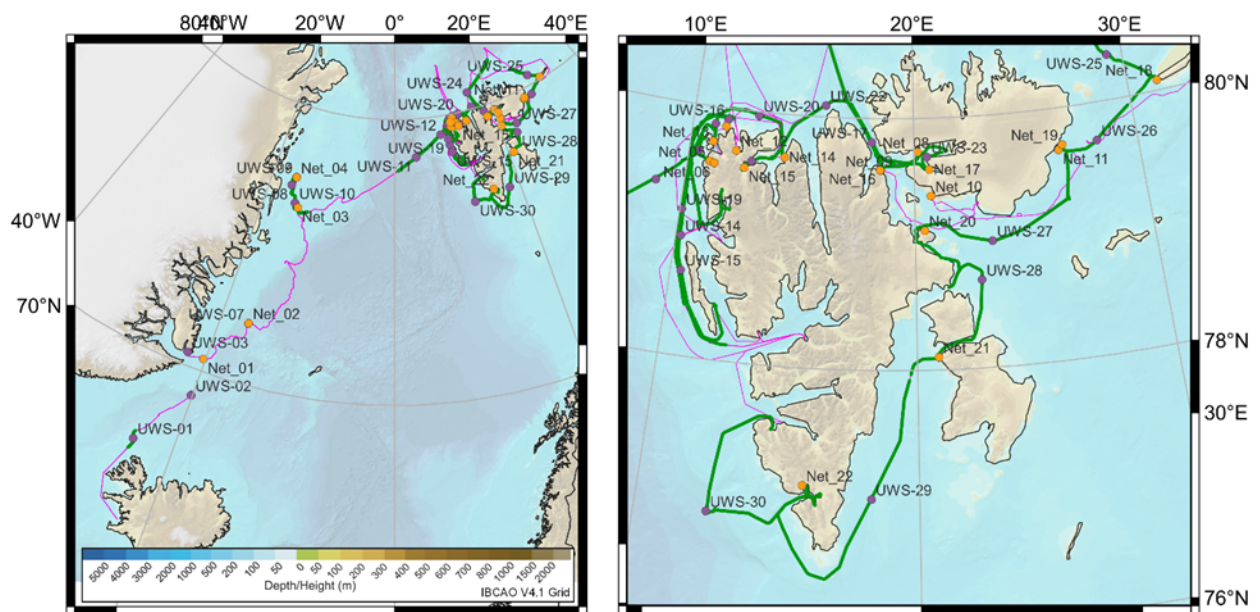


**Fig. 6.1.** Cruise track, and UWS and NET sample stations. The magenta line indicates the cruise track. Missing sections are where the thermosalinograph and GPS were turned off due to ice clogging the seawater intake. Green lines and purple dots indicate the full sampling track and midpoint of UWS samples. Orange dots indicate NET locations.

Particles floating at the sea surface were collected with a manta net (NET) with an opening of 20 x 60 cm and a mesh size of 300  $\mu\text{m}$ . A total of 22 NET stations were sampled. At stations where floating sea ice was unavoidable, the net opening was protected from large ice pieces with a  $\sim$ 4 cm mesh steel grid. The net was extended away from the boat wake on a lateral boom. Three net tows were conducted at each net station for 15-20 min each at a speed of approximately 4 knots, representing a tow length of  $1460 \pm 240$  m, or an area of  $\sim$ 900 m<sup>2</sup>. Track lengths were continuously recorded by GPS and used to calculate exact tow lengths. Track positions were not identical replicates, but were chosen to provide as representative coverage of a site as possible (e.g., offshore vs. nearshore, shore-parallel vs. shore-normal, fjord shore vs. glacier front, etc.).

After each tow, the net interior was thoroughly washed into the cod-end by repeated and vigorous dipping while the net mouth was out of the water. The cod-end was removed and placed in a stainless-steel container with tight-fitting lid, and replaced with a new cod-end. On return to the ship's laboratory, the cod ends were rinsed into a stainless-steel 300  $\mu\text{m}$  sieve and transferred to 500 mL swing-top glass jars. Particles were visually identified under a dissecting scope or magnifying glass; all apparently non-natural particles were selected for imaging, as well as a representative selection of natural particles (e.g., amphipods, macroalgae, bird feathers, wood fragments, etc.).

Microplastic polymer types were identified using a near-infrared (NIR) hyperspectral imaging system. The hyperspectral imaging system used in the current study was a Specim FX17 camera (Specim Spectral Imaging Ltd.; Oulu, Finland) mounted on a Specim linear lab bed scanner. The FX17 linescan camera has a spectral range of 900 – 1700 nm, with 224 spectral bands and spatial sampling of 640 pixels. A macro lens was used to achieve a field of view of about 1200  $\mu\text{m}$ , giving a pixel dimension of approximately 2-4  $\mu\text{m}$ . Dry particles were mounted on a black, non-reflective slide and illuminated overhead by two halogen lights at approximately 45°C from the front and back of the camera target field. The hyperspectral camera and lab scanner were controlled using Specim's LUMO software suite.

A combination of an edge-finding algorithm (Sobel) and a segmentation algorithm (Watershed) from Scikit-image (van der Walt et al., 2014), were used to identify particles in the images. Particle dimensions were calculated according to the calibrated pixel size. NIR spectra were averaged over the identified particle area. The Scikit-learn random forest algorithm (Pedregosa et al., 2011) was used to classify the particle polymer types based on this average spectral signature. The algorithm was trained and validated using more than 100k spectra obtained from a range of household plastic objects. The polymers in the training set included polystyrene (PS), polyvinyl chloride (PVC), high- and low-density polyethylene (HDPE and LDPE), polyethylene terephthalate (PET), and polypropylene (PP). Polyethylene was grouped as a single type because the NIR spectra for high-

and low-density PE are identical. The spectra for plastic polymers are markedly different from those for natural materials.

Macroplastic debris was manually collected from the pack ice surface near the Greenland village of Ittoqqortoormiit and along shorelines in Svalbard (e.g., Figs. 2 and 3). Small subsamples (~0.5 cm<sup>2</sup>) were cut from the microplastic objects for NIR imaging and polymer identification.



**Fig. 6.2.** Examples of macroplastic debris found on the pack ice near the Greenland village of Ittoqqortoormiit.



**Fig. 6.3.** Examples of macroplastic debris found on the shorelines around Svalbard.

### **Preliminary Results and Discussion**

No plastic particles were found in the UWS samples, even at stations where the ship was stationary and manta trawls indicated a high abundance of microplastic particles at the sea surface. Instead, UWS samples throughout the study area consisted almost entirely of copepods, with some pteropods. The presence of pteropods  $>300\ \mu\text{m}$  in surface waters is consistent with previous studies in the region (e.g., Anglada-Ortiz et al., 2021). Some transparent, film-like particles were found which appeared similar to clear plastics, but their NIR spectra were identical to intact copepods, suggesting that they were shell fragments from large copepods or amphipods. The lack of MPs in UWS samples indicates that large MP particles float very close to the sea surface, in contrast to small particles which can be found throughout the water column (e.g., Pabortsava and Lampitt, 2020).

Microplastic particles were more abundant in the manta net samples (e.g., Fig. 4), with MPs detected in 32 of the 66 individual net tows, and at all but five stations (Fig. 5). At stations 1 (NW of Iceland), 6 (W of Svalbard), 11, 12, and 18 (all NNE Svalbard), no MPs were detected in any of the triplicate net tows. Along the Greenland coast, 50% of the tows contained no detected MPs and the other 50% contained one or two particles per tow, representing 10-25 MPs per km<sup>2</sup>. Net-collected MPs around Svalbard also showed highly variable abundances, but were much higher, averaging 60 MP/km<sup>2</sup> and ranged as high as 1220 MP/km<sup>2</sup>.





**Fig. 6.4.** Floating debris collected in the manta net, with abundant microplastic particles evident. (L) Station Net-16, (R) Station Net-19.

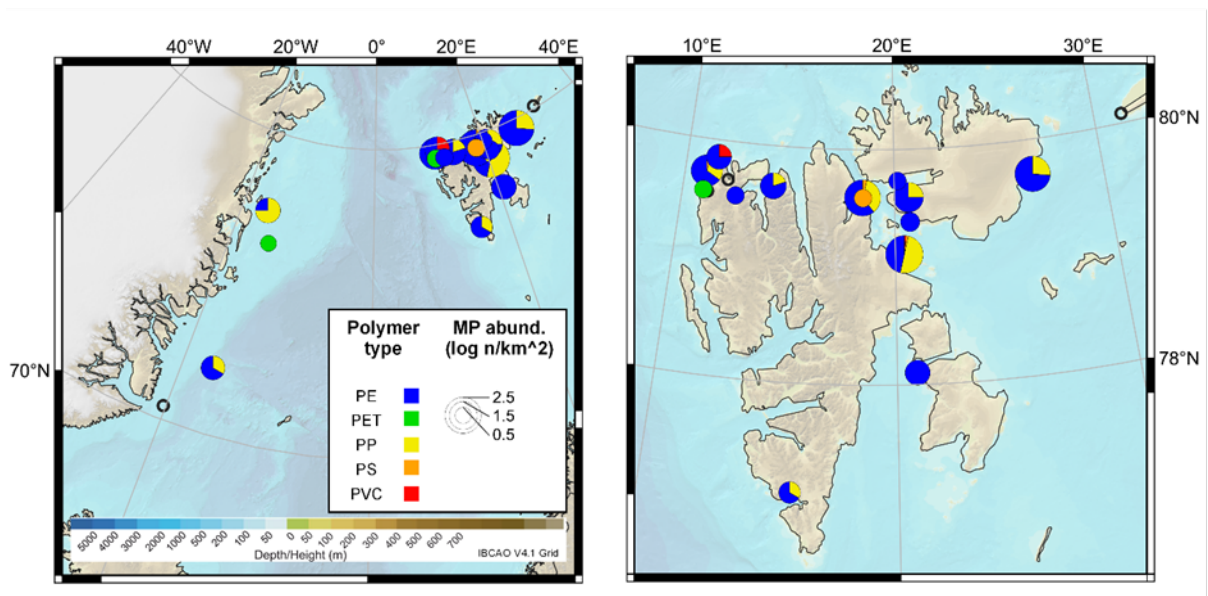


**Fig. 6.5.** Distribution, abundance, and polymer type of net-collected microplastics. The right-hand panel shows a zoomed-in view around Svalbard. MP abundance is shown by the symbol size (note that these are log-scaled, i.e., circle size 1 = 10 MP/km<sup>2</sup>). Stations where no MP were found are indicated by hollow black circles.

The high variability in net-collected MPs was evident not just among stations, but also within individual stations. For example, net tows 47, 48, and 49 (station “Net\_16”) collected 660, 170, and 30 particles/km<sup>2</sup>, respectively. This is likely due in part to the sampling strategy, in which the three tows at each station were not replicates in a strict sense, but represent the variability within each site. The variable abundances are also due to small-scale heterogeneity in MP accumulation due to local winds and currents. Accumulation of floating debris along Langmuir circulation and formation of windrows was clearly evident at some sites (e.g., Fig. 6). These windrows can greatly concentrate floating materials such as MPs (Thorpe, 2009; Hamner and Schneider, 1986; Van Sebille et al., 2020), and can appear and disappear on time scales shorter than a single net tow (Thorpe, 2004). Where the net tow path crossed a windrow, much higher MP abundances were observed.

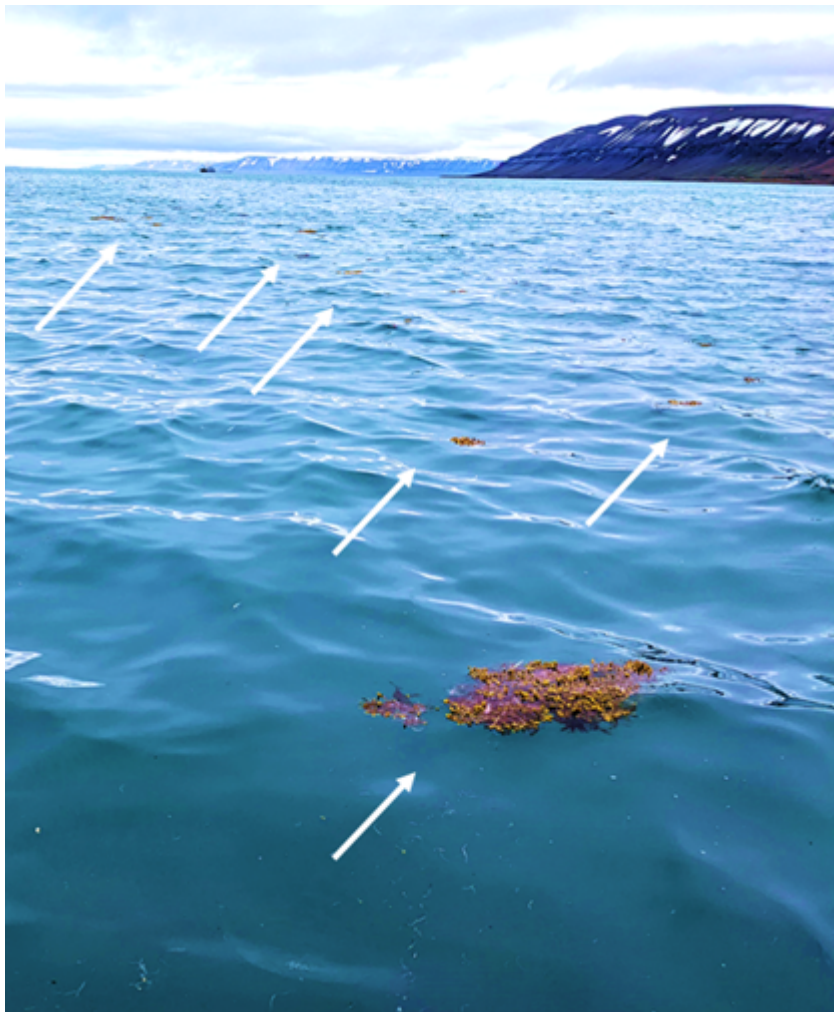


**Fig. 6.6.** *Floating debris accumulation along a windrow at Station Net-21. Arrows indicate macroalgae clumps, and smaller particles are visible at the bottom of the image. (Note: colors in the image have been oversaturated to increase contrast.)*

The net-collected MP polymer types were dominated by PE (58.9%) and PP (37.4%) (Fig. 7). The third most abundant polymer was PS (2.3%), and PVC and PET each represented less than 1% (Fig. 7). The high prevalence of PE and PP in the floating MP pool is unsurprising given their low

density compared to seawater ( $<1 \text{ g/cm}^3$ ), and these polymers were also the most abundant observed in local macroplastic debris. This further suggests that microplastics may be derived from fragmentation of local macroplastics. The polymers PS and PET were not detected in microplastic debris. Significant detection of floating PS microplastics is less expected than for PE and PP, but most of the PS particles appeared similar to foamed PS typically used in rigid insulating material (Fig. 8), which has a very low density ( $<0.1 \text{ g/cm}^3$ ).

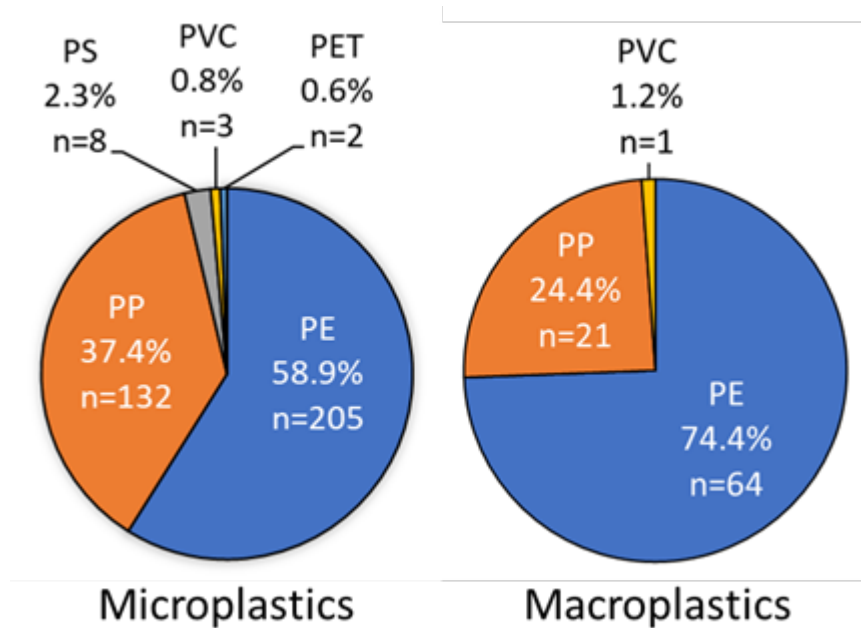


**Fig. 6.7.** Proportion of polymer types detected in the net-collected microplastic particles and microplastic debris collected from shore. "n" indicates the total number of particles or samples of each type collected.



**Fig. 6.8.** Apparent foamed polystyrene particle, 7.5 x 4 mm. Collected at station Net-13.

Most of the MP particles collected in the current study were between 1 and 4 mm, with an approximately exponential increase with decreasing size to 1 mm. Lower MP abundances were observed below 0.5 and 1 mm (Fig. 9a). The decrease in abundance at small sizes has been documented for net-collected microplastics (e.g., Lindeque et al., 2020), and is likely due to loss of particles according to their smallest dimension. This is evident in the higher abundance of particles with secondary diameter less than 1 mm (Fig. 9a), and the length-to-width ratios greater than 1 (Fig. 9b). Low abundance of small size classes may also be an undersampling artefact due to the manual picking method without digestion.

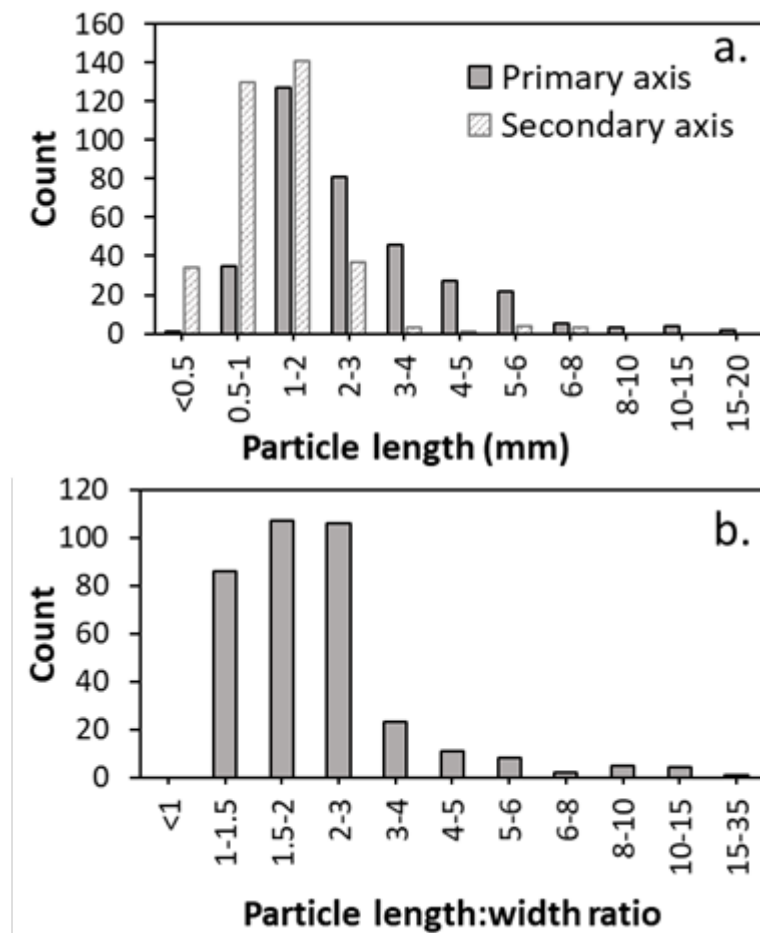


**Fig. 6.9.** Microplastic particle dimensions (a) length, (b) length:width ratio.

The length:width ratio of collected MPs was mostly constrained to a relatively narrow range between 1 and 4 (Fig. 9b). High ratios are indicative of long, fiber-like particles, and indeed, the highest ratios clearly were associated with rope-like material. The relative lack of large fibers is striking considering the abundance of plastic ropes and net debris nearly ubiquitous on Svalbard shorelines (Fig. 3). The most abundant macroplastics on the sea ice near Ittoqqortoormiit were films or bags (Fig. 2), and such thin, flexible particles were also not common in the samples.

The apparent disconnect between local microplastic debris and microplastics suggests either that most of the collected microplastics originate elsewhere, or that the fragmentation lifetime of plastic films and ropes is short. Net collection would miss fragments smaller than the net mesh (Lindeque et al., 2020). Alternatively, microplastic weathering on beaches may be decoupled from microplastics in the water column (Andrady, 2022).

## 7 Overview of stations and sampling activities

**Table 7.1:** Overview of all stations and sampling activities. Niskin samples were used for measurements of dissolved oxygen (using Winkler titration), chlorophyll *a* and other phytoplankton pigments (using HPLC), as well as particulate organic carbon and nitrogen (POC/PON). Depending on water availability, not all parameters could be sampled at every station. The total amount of samples was 88 (O<sub>2</sub>), 107 (Chl *a* / pigments), and 115 (POC/PON). Data availability from vertical profiles with CTD and UVP6 are denoted by yes/no (y/n), and were always conducted to the maximum depth of Niskin sampling. Note that the UVP6 was only available for cruise legs 1 & 2.

Cruise leg	Station #	time (CEST)	Lat N (minutes/secs)	Lon E (minutes/secs)	Niskin depth (m)	CTD	UVP6
1	1	2022-06-04 21:30:00	68°04'03.26"	022°18'02.00"	30	n	n
1	2	2022-06-05 05:30:00	69°02'08.87"	020°13'38.74"	30	n	y
1	2	2022-06-05 05:30:00	69°02'08.87"	020°13'38.74"	50	n	y
1	2	2022-06-05 05:30:00	69°02'08.87"	020°13'38.74"	100	n	y
1	2	2022-06-05 05:30:00	69°02'08.87"	020°13'38.74"	250	n	y
1	2	2022-06-05 05:30:00	69°02'08.87"	020°13'38.74"	250	n	y
1	3	2022-06-05 19:00:00	70°17.913'	021°27.995'	30	y	y
1	3	2022-06-05 19:00:00	70°17.913'	021°27.995'	50	y	y
1	3	2022-06-05 19:00:00	70°17.913'	021°27.995'	100	y	y
1	3	2022-06-05 19:00:00	70°17.913'	021°27.995'	250	y	y
1	4	2022-06-06 17:00:00	70°26.6101'	02°3.1587'	10	y	y
1	4	2022-06-06 17:00:00	70°26.6101'	02°3.1587'	20	y	y
1	4	2022-06-06 17:00:00	70°26.6101'	02°3.1587'	70	y	y
1	5	2022-06-08 14:00:00	72°06'44.65"	016°50'56.93"	20	y	y
1	5	2022-06-08 14:00:00	72°06'44.65"	016°50'56.93"	30	y	y
1	5	2022-06-08 14:00:00	72°06'44.65"	016°50'56.93"	50	y	y
1	5	2022-06-08 14:00:00	72°06'44.65"	016°50'56.93"	250	y	y
1	5	2022-06-08 14:00:00	72°06'44.65"	016°50'56.93"	900	y	y
1	6	2022-06-09 14:30:00	74°28'50.95"	014°32'06.09"	30	y	y
1	6	2022-06-09 14:30:00	74°28'50.95"	014°32'06.09"	60	y	y
1	6	2022-06-09 14:30:00	74°28'50.95"	014°32'06.09"	120	y	y
1	6	2022-06-09 14:30:00	74°28'50.95"	014°32'06.09"	200	y	y
1	7	2022-06-10 14:00:00	76°27'12.18"	014°44'55.52"	30	y	y
1	7	2022-06-10 14:00:00	76°27'12.18"	014°44'55.52"	60	y	y
1	7	2022-06-10 14:00:00	76°27'12.18"	014°44'55.52"	120	y	y
1	7	2022-06-10 14:00:00	76°27'12.18"	014°44'55.52"	180	y	y

1	8	2022-06-11 07:00:00	77°29'54.94"	016°07'00.33"	30	y	y
1	8	2022-06-11 07:00:00	77°29'54.94"	016°07'00.33"	60	y	y
1	8	2022-06-11 07:00:00	77°29'54.94"	016°07'00.33"	120	y	y
1	8	2022-06-11 07:00:00	77°29'54.94"	016°07'00.33"	200	y	y
1	10	2022-06-12 11:30:00	77°23.9260'	005°04.0213'	30	y	y
1	10	2022-06-12 11:30:00	77°23.9260'	005°04.0213'	130	y	y
1	10	2022-06-12 11:30:00	77°23.9260'	005°04.0213'	230	y	y
1	10	2022-06-12 11:30:00	77°23.9260'	005°04.0213'	530	y	y
1	11	2022-06-13 02:00:00	79°03.8901'	006°47.6040'	30	y	y
1	11	2022-06-13 02:00:00	79°03.8901'	006°47.6040'	130	y	y
1	11	2022-06-13 02:00:00	79°03.8901'	006°47.6040'	230	y	y
1	11	2022-06-13 02:00:00	79°03.8901'	006°47.6040'	530	y	y
2	14	2022-06-16 08:00:00	79°47'37.73"	010°05'35.60"	5	y	y
2	14	2022-06-16 08:00:00	79°47'37.73"	010°05'35.60"	30	y	y
2	14	2022-06-16 08:00:00	79°47'37.73"	010°05'35.60"	130	y	y
2	14	2022-06-16 08:00:00	79°47'37.73"	010°05'35.60"	230	y	y
2	14	2022-06-16 08:00:00	79°47'37.73"	010°05'35.60"	350	y	y
2	15	2022-06-17 00:30:00	80°06'39.95"	017°07'36.22"	5	y	y
2	15	2022-06-17 00:30:00	80°06'39.95"	017°07'36.22"	30	y	y
2	15	2022-06-17 00:30:00	80°06'39.95"	017°07'36.22"	130	y	y
2	15	2022-06-17 00:30:00	80°06'39.95"	017°07'36.22"	100	y	y
2	15	2022-06-17 00:30:00	80°06'39.95"	017°07'36.22"	230	y	y
2	17	2022-06-19 01:00:00	79°11'06.78"	025°31'16.05"	5	y	y
2	17	2022-06-19 01:00:00	79°11'06.78"	025°31'16.05"	30	y	y
2	17	2022-06-19 01:00:00	79°11'06.78"	025°31'16.05"	50	y	y
2	17	2022-06-19 01:00:00	79°11'06.78"	025°31'16.05"	120	y	y
2	17	2022-06-19 01:00:00	79°11'06.78"	025°31'16.05"	160	y	y
2	19	2022-06-20 02:30:00	80°42'59.50"	029°47'16.92"	5	y	y
2	19	2022-06-20 02:30:00	80°42'59.50"	029°47'16.92"	30	y	y
2	19	2022-06-20 02:30:00	80°42'59.50"	029°47'16.92"	100	y	y
2	19	2022-06-20 02:30:00	80°42'59.50"	029°47'16.92"	200	y	y
2	19	2022-06-20 02:30:00	80°42'59.50"	029°47'16.92"	410	y	y
2	20	2022-06-20 22:30:00	79°50'28.10°	014°05'21.13"	5	y	y
2	20	2022-06-20 22:30:00	79°50'28.10°	014°05'21.13"	30	y	y
2	20	2022-06-20 22:30:00	79°50'28.10°	014°05'21.13"	50	y	y
2	20	2022-06-20 22:30:00	79°50'28.10°	014°05'21.13"	80	y	y
2	20	2022-06-20 22:30:00	79°50'28.10°	014°05'21.13"	110	y	y
2	21	2022-06-22 01:50:00	79°02'28.50"	010°51.30.06"	5	y	y
2	21	2022-06-22 01:50:00	79°02'28.50"	010°51.30.06"	30	y	y
2	21	2022-06-22 01:50:00	79°02'28.50"	010°51.30.06"	50	y	y
2	21	2022-06-22 01:50:00	79°02'28.50"	010°51.30.06"	80	y	y
2	21	2022-06-22 01:50:00	79°02'28.50"	010°51.30.06"	110	y	y
3	22	2022-06-24 10:00:00	79°33'49.94"N	010° 59'41.39"E	5	y	n
3	22	2022-06-24 10:00:00	79°33'49.94"N	010° 59'41.39"E	20	y	n
3	22	2022-06-24 10:00:00	79°33'49.94"N	010° 59'41.39"E	40	y	n
3	22	2022-06-24 10:00:00	79°33'49.94"N	010° 59'41.39"E	60	y	n
3	22	2022-06-24 10:00:00	79°33'49.94"N	010° 59'41.39"E	70	y	n

*Le Commandant Charcot, Reykjavik -- Longyearbyen, 3 June 2022 – 8 July 2022*

3	23	2022-06-25 14:00:00	81°46'55.99"N	009° 58'17.68"E	25	y	n
3	23	2022-06-25 14:00:00	81°46'55.99"N	009° 58'17.68"E	215	y	n
3	23	2022-06-25 14:00:00	81°46'55.99"N	009° 58'17.68"E	415	y	n
3	23	2022-06-25 14:00:00	81°46'55.99"N	009° 58'17.68"E	615	y	n
3	23	2022-06-25 14:00:00	81°46'55.99"N	009° 58'17.68"E	765	y	n
3	24	2022-06-27 04:30:00	78°56'04.69"N	011° 55'55.40"E	5	y	n
3	24	2022-06-27 04:30:00	78°56'04.69"N	011° 55'55.40"E	30	y	n
3	24	2022-06-27 04:30:00	78°56'04.69"N	011° 55'55.40"E	130	y	n
3	24	2022-06-27 04:30:00	78°56'04.69"N	011° 55'55.40"E	230	y	n
3	24	2022-06-27 04:30:00	78°56'04.69"N	011° 55'55.40"E	310	y	n
4	25	2022-06-22 01:47:00	79° 50' 54.88"	10° 20' 9.33"	10	y	n
4	25	2022-06-22 01:47:00	79° 50' 54.88"	10° 20' 9.33"	30	y	n
4	25	2022-06-22 01:47:00	79° 50' 54.88"	10° 20' 9.33"	130	y	n
4	25	2022-06-22 01:47:00	79° 50' 54.88"	10° 20' 9.33"	230	y	n
4	25	2022-06-22 01:47:00	79° 50' 54.88"	10° 20' 9.33"	300	y	n
4	26	2022-07-01 03:32:00	79° 52'52.85"	17° 54'15.94"	395	y	n
4	26	2022-07-01 03:32:00	79° 52'52.85"	17° 54'15.94"	385	y	n
4	26	2022-07-01 03:32:00	79° 52'52.85"	17° 54'15.94"	275	y	n
4	26	2022-07-01 03:32:00	79° 52'52.85"	17° 54'15.94"	10	y	n
4	26	2022-07-01 03:32:00	79° 52'52.85"	17° 54'15.94"	125	y	n
4	27	2022-07-02 14:52:00	81° 52'52.79"N	23° 0'53.26"E	850	y	n
4	27	2022-07-02 14:52:00	81° 52'52.79"N	23° 0'53.26"E	730	y	n
4	27	2022-07-02 14:52:00	81° 52'52.79"N	23° 0'53.26"E	580	y	n
4	27	2022-07-02 14:52:00	81° 52'52.79"N	23° 0'53.26"E	430	y	n
4	27	2022-07-02 14:52:00	81° 52'52.79"N	23° 0'53.26"E	280	y	n
4	27	2022-07-02 14:52:00	81° 52'52.79"N	23° 0'53.26"E	130	y	n
4	27	2022-07-02 14:52:00	81° 52'52.79"N	23° 0'53.26"E	30	y	n
4	27	2022-07-02 14:52:00	81° 52'52.79"N	23° 0'53.26"E	10	y	n
4	28	2022-07-03 03:47:00	80° 21.391'N	029°23.127"E	400	y	n
4	28	2022-07-03 03:47:00	80° 21.391'N	029°23.127"E	280	y	n
4	28	2022-07-03 03:47:00	80° 21.391'N	029°23.127"E	130	y	n
4	28	2022-07-03 03:47:00	80° 21.391'N	029°23.127"E	30	y	n
4	28	2022-07-03 03:47:00	80° 21.391'N	029°23.127"E	10	y	n
4	29	2022-07-03 23:18:00	79° 16'19.92"N	026° 35'40.76"E	230	y	n
4	29	2022-07-03 23:18:00	79° 16'19.92"N	026° 35'40.76"E	160	y	n
4	29	2022-07-03 23:18:00	79° 16'19.92"N	026° 35'40.76"E	110	y	n
4	29	2022-07-03 23:18:00	79° 16'19.92"N	026° 35'40.76"E	30	y	n
4	29	2022-07-03 23:18:00	79° 16'19.92"N	026° 35'40.76"E	10	y	n
4	30	2022-07-06 05:39:00	76° 58'32.21"N	015° 44'49.03"E	220	y	n
4	30	2022-07-06 05:39:00	76° 58'32.21"N	015° 44'49.03"E	10	y	n
4	30	2022-07-06 05:39:00	76° 58'32.21"N	015° 44'49.03"E	100	y	n
4	30	2022-07-06 05:39:00	76° 58'32.21"N	015° 44'49.03"E	30	y	n

## 7.2 Microplastic sampling

**Table 7.2:** Underway sampling for microplastics

Sample ID	Transect	Date_time	Vol_m <sup>3</sup>	Longitude (W)	Latitude (N)
UWS-01	Start	04/06/2022 12:00	5.03	-23.715011	66.64393
	End	04/06/2022 16:00		-23.703177	67.271051
UWS-02	Start	05/06/2022 05:00	2.22	-20.226358	69.035981
	End	05/06/2022 09:00		-20.222963	69.180363
UWS-03	Start	06/06/2022 09:00	8.34	-22.006591	70.469533
	End	06/06/2022 21:46		-22.00657	70.469533
UWS-04	Start	06/06/2022 21:46	7.28	-22.006566	70.469536
	End	07/06/2022 08:40		-22.006592	70.469539
UWS-05	Start	07/06/2022 08:40	3.87	-22.006592	70.469539
	End	07/06/2022 13:00		-22.006571	70.469531
UWS-07	Start	08/06/2022 14:10	2.63	-16.83169	72.109341
	End	08/06/2022 18:00		-16.782526	72.099924
UWS-08	Start	10/06/2022 19:35	6.00	-16.078439	76.854949
	End	11/06/2022 03:45		-16.111944	77.499934
UWS-09	Start	11/06/2022 09:00	1.63	-16.109276	77.500649
	End	11/06/2022 12:00		-16.159274	77.437431
UWS-10	Start	11/06/2022 13:30	2.85	-16.189427	77.067276
	End	11/06/2022 19:45		-13.144646	76.396072
UWS-11	Start	12/06/2022 18:47	4.10	0.553837	78.189959
	End	13/06/2022 01:35		6.401225	79.004086
UWS-12	Start	13/06/2022 01:35	4.04	6.405571	79.004914
	End	13/06/2022 07:50		10.995051	79.563938
UWS-13	Start	13/06/2022 07:55	7.83	10.995088	79.564009
	End	13/06/2022 21:30		10.618393	79.737022
UWS-14	Start	13/06/2022 21:35	8.81	10.617241	79.737176



*Le Commandant Charcot, Reykjavik -- Longyearbyen, 3 June 2022 – 8 July 2022*

	End	14/06/2022 09:41		12.008325	78.422694
UWS-15	Start	15/06/2022 20:05	10.80	12.589739	78.132832
	End	16/06/2022 09:50		11.554987	79.878237
UWS-16	Start	16/06/2022 10:55	9.15	11.532219	79.857007
	End	16/06/2022 17:35		11.577939	79.941298
UWS-17	Start	16/06/2022 23:30	8.52	17.13861	80.10995
	End	17/06/2022 11:10		20.211002	79.759837
UWS-18	Start	21/06/2022 11:25	20.15	11.804475	79.923818
	End	22/06/2022 12:10		12.081809	79.201
UWS-19	Start	29/06/2022 18:00	4.55	10.761345	78.41162
	End	30/06/2022 01:00		10.673791	79.900054
UWS-20	Start	30/06/2022 01:00	4.91	10.695786	79.902584
	End	30/06/2022 10:50		14.131821	79.671285
UWS-21	Start	30/06/2022 11:15	4.34	13.620971	79.64061
	End	30/06/2022 18:42		13.395228	79.639124
UWS-22	Start	30/06/2022 19:00	9.08	13.685827	79.650762
	End	01/07/2022 11:45		20.634182	79.576238
UWS-23	Start	01/07/2022 12:15	3.95	20.652186	79.572677
	End	01/07/2022 17:58		21.248434	79.726377
UWS-24	Start	01/07/2022 18:15	4.92	21.445522	79.735744
	End	02/07/2022 07:00		22.660788	81.475099
UWS-25	Start	02/07/2022 23:00	5.33	26.891645	80.839476
	End	03/07/2022 11:50		30.030103	79.958491
UWS-26	Start	03/07/2022 12:00	4.03	29.819757	79.931562
	End	03/07/2022 21:40		26.582249	79.273561
UWS-27	Start	03/07/2022 22:00	6.04	26.546472	79.275151
	End	04/07/2022 11:55		20.080538	79.019538
UWS-28	Start	04/07/2022 12:00	10.95	20.129541	79.016551

	End	05/07/2022 17:50		19.740348	77.969179
UWS-29	Start	05/07/2022 18:00	7.79	19.678166	77.923491
	End	06/07/2022 11:45		15.978374	77.071186
UWS-30	Start	06/07/2022 12:00	7.77	15.982881	77.0681
	End	07/07/2022 07:30		14.554912	77.500959

**Table 7.3:** Manta Net sampling stations for microplastics

Station	Date_time	Track_length (m)	Longitude (W)	Latitude (N)
Net_1	07/06/2022 21:10	1308.19	-20.2407	70.4356
Net_2	08/06/2022 13:23	1337.535	-16.81839	72.10785
Net_3	10/06/2022 13:33	1513.875	-14.7584	76.46469
Net_4	11/06/2022 04:47	1469.698	-16.16667	77.48078
Net_5	13/06/2022 06:45	1389.228	10.97169	79.56429
Net_6	13/06/2022 12:27	1421.208	11.185	79.55433
Net_7	16/06/2022 11:58	1142.406	11.51426	79.85479
Net_8	17/06/2022 06:12	1273.026	20.15316	79.73334
Net_9	17/06/2022 15:21	1427.649	18.51511	79.5884
Net_10	18/06/2022 11:46	1529.59	20.70036	79.38269
Net_11	19/06/2022 06:56	1548.556	26.43201	79.6681
Net_12	21/06/2022 05:59	1549.76	12.08199	79.67348
Net_13	21/06/2022 13:42	1493.728	11.01974	79.72516
Net_14	30/06/2022 06:39	1379.684	14.24502	79.65879
Net_15	30/06/2022 13:31	1327.526	12.51147	79.54665
Net_16	01/07/2022 06:32	1445.968	18.49192	79.59107
Net_17	01/07/2022 12:31	1711.315	20.65983	79.59265
Net_18	03/07/2022 06:45	1460.139	31.36258	80.08212

*Le Commandant Charcot, Reykjavik -- Longyearbyen, 3 June 2022 – 8 July 2022*

---

Net_19	03/07/2022 15:31	1754	26.621	79.70562
Net_20	04/07/2022 06:54	1534.941	20.39954	79.10839
Net_21	05/07/2022 12:02	1387.745	20.82556	78.10186
Net_22	06/07/2022 06:28	1644.575	15.82095	77.07363

## 8 Data and Sample Storage and Availability

**Table 8.1** Overview of data availability

Type	Database	Available	Free Access	Contact
CTD hydrography (raw data)	OSIS	6/2023	1/2024	aoschlies@geomar.de, jtaucher@geomar.de
Dissolved O <sub>2</sub>	PANGAEA	6/2023	1/2024	aoschlies@geomar.de, jtaucher@geomar.de
Chlorophyll <i>a</i> and other pigments	PANGAEA	6/2023	1/2024	aoschlies@geomar.de, jtaucher@geomar.de
POC & PON	PANGAEA	6/2023	1/2024	aoschlies@geomar.de, jtaucher@geomar.de
UVP6 particles & zooplankton	EcoTaxa	6/2023	1/2024	jtaucher@geomar.de
Microplastic concentration and polymer type	EMODnet	6/2023	1/2024	ajbeck@geomar.de

**Table 8.2.** Summary data table, net-collected microplastic particles.

Station	Date	Track length <sup>a</sup> (m)	Longitude	Latitude	Total MP <sup>b</sup>	Average MP (#/km <sup>2</sup> )	± MP (1 S.D.) (#/km <sup>2</sup> )	log MP	# MP per polymer type				
									PVC	PS	PP	PET	PE
Net 1	07/06/2022	1340	-20.241	70.436	0	0.0	0.0	0	0	0	0	0	0
Net 2	08/06/2022	1453	-16.818	72.108	3	11.8	12.5	1.1	0	0	1	0	2
Net 3	10/06/2022	1655	-14.758	76.465	1	3.0	5.2	0.5	0	0	0	1	0
Net 4	11/06/2022	1418	-16.167	77.481	4	15.9	7.6	1.2	0	0	3	0	1
Net 5	13/06/2022	1392	10.972	79.564	1	3.9	6.8	0.6	0	0	0	1	0
Net 6	13/06/2022	1137	11.185	79.554	0	0.0	0.0	0	0	0	0	0	0
Net 7	16/06/2022	1436	11.514	79.855	4	16.4	14.9	1.2	1	0	0	0	3
Net 8	17/06/2022	1304	20.153	79.733	1	4.4	7.6	0.6	0	0	0	0	1
Net 9	17/06/2022	1445	18.515	79.588	1	3.8	6.5	0.6	0	1	0	0	0
Net 10	18/06/2022	1342	20.700	79.383	1	4.8	8.3	0.7	0	0	0	0	1
Net 11	19/06/2022	1425	26.432	79.668	0	0.0	0.0	0	0	0	0	0	0
Net 12	21/06/2022	1344	12.082	79.673	0	0.0	0.0	0	0	0	0	0	0
Net 13	21/06/2022	1298	11.020	79.725	20	86.7	98.1	1.9	0	1	6	0	13
Net 14	30/06/2022	1433	14.245	79.659	5	18.7	18.2	1.3	0	0	1	0	4
Net 15	30/06/2022	1481	12.511	79.547	1	4.4	7.7	0.6	0	0	0	0	1
Net 16	01/07/2022	1369	18.492	79.591	74	285.2	329.8	2.5	0	3	26	0	45
Net 17	01/07/2022	1497	20.660	79.593	12	46.1	41.9	1.7	0	0	3	0	9
Net 18	03/07/2022	1592	31.363	80.082	0	0.0	0.0	0	0	0	0	0	0
Net 19	03/07/2022	1645	26.621	79.706	76	262.6	383.6	2.4	0	0	20	0	56
Net 20	04/07/2022	1511	20.400	79.108	142	516.5	609.5	2.7	2	3	71	0	66
Net 21	05/07/2022	1812	20.826	78.102	6	17.7	19.7	1.2	0	0	0	0	6
Net 22	06/07/2022	1821	15.821	77.074	3	8.5	8.0	0.9	0	0	1	0	2

<sup>a</sup> Track length, average of three tows.

<sup>b</sup> Total number of MP collected in three tows at each site.

## **9 Acknowledgements**

We greatly appreciate the assistance on all fronts from the ship's crew, especially the Captain and Chief Engineer. This work would not have been possible without the enthusiastic and tireless efforts and expertise of the ship's Science Coordinators, Daniel Cron and Daphné Buiron. Financial travel support for this work was provided by Ponant, and analytical support from GEOMAR Helmholtz Centre for Ocean Research Kiel.

## **10 References**

Anglada-Ortiz, G., Zamelczyk, K., Meilland, J., Ziveri, P., Chierici, M., Fransson, A., & Rasmussen, T. L. (2021). Planktic foraminiferal and pteropod contributions to carbon dynamics in the Arctic Ocean (North Svalbard Margin). *Frontiers in Marine Science*, 8, 636.

Andrady, A. L. (2022). Weathering and fragmentation of plastic debris in the ocean environment. *Marine Pollution Bulletin*, 180, 113761.

Thorpe, S. A. (2004). Langmuir circulation. *Annual Review of Fluid Mechanics*, 36(1), 55-79.

Thorpe, S. A. (2009). Spreading of floating particles by Langmuir circulation. *Marine Pollution Bulletin*, 58(12), 1787-1791.

Hamner, W. M., & Schneider, D. (1986). Regularly spaced rows of medusae in the Bering Sea: Role of Langmuir circulation 1. *Limnology and Oceanography*, 31(1), 171-176.

Van Sebille, E., Aliani, S., Law, K. L., Maximenko, N., Alsina, J. M., Bagaev, A., ... & Wichmann, D. (2020). The physical oceanography of the transport of floating marine debris. *Environmental Research Letters*, 15(2), 023003.

Pabortsava, K., & Lampitt, R. S. (2020). High concentrations of plastic hidden beneath the surface of the Atlantic Ocean. *Nature communications*, 11(1), 1-11.

Picheral 2021 - The Underwater Vision Profiler 6- an imaging sensor of particle size spectra and plankton, for autonomous and cabled platforms

Lindeque, P. K., Cole, M., Coppock, R. L., Lewis, C. N., Miller, R. Z., Watts, A. J., ... & Galloway, T. S. (2020). Are we underestimating microplastic abundance in the marine environment? A comparison of microplastic capture with nets of different mesh-size. *Environmental Pollution*, 265, 114721.